Wind Turbine Team at Virginia Tech

Technical Design Written Report

2019 U.S. Department of Energy Collegiate Wind Competition

Virginia Polytechnic Institute and State University

Kevin T. Crofton Department of Aerospace and Ocean Engineering

Blacksburg, Virginia, (540) 231-6611, WindTurbineTeamVT@vt.edu

www.vtwtt.aoe.vt.edu, Twitter/Instagram/Facebook: @WindTurbineTeamVT

Team Leaders

Jonathan Hawes (Technical Lead) | **Adham Nabhan** (Project Manager)

Laura Burger (Siting) | **Chris Miller and Drew Richard** (Mechanical)

Minh Ngo (Power Systems and Controls) | **Alex McLean** (Blade)

Advisors

Dr. Matthew Kuester (Principal Investigator, Department of Aerospace Engineering)

Dr. Arthur Ball (Assistant Investigator, Department of Electrical Engineering)

Members: 52 (9 majors), Advisors: 2

COLLEGIATE WIND COMPETITION
U.S. DEPARTMENT OF ENERGY

VIRGINIA TECH

Table of Contents

Executive Summary

In designing a wind turbine for the 2019 Collegiate Wind Competition in Boulder, Colorado, the Wind Turbine Team at Virginia Tech focused on developing a design that could accomplish the competition tasks as simply and effectively as possible, even in operational extremes.

The overall design of the turbine, shown in **Figure 1**, began with the blades, which were designed to provide the most power possible at low wind speeds while still having a high rated power. MATLAB code was developed to simulate the performance of the blades at all operational modes, in combination with the open-source software QBlade. To be able to control the turbine for the Control of Rated Power and Speed and Durability Tasks more effectively, a mechanical pitch control system was developed that focused on precision, reliability, and low power consumption. With a precision of half a degree of rotation and 75 degrees of total movement of the blades, the blades can be effectively pitched using a stepper motor to the necessary angle to either maintain rated power, or to find maximum power possible during the Power Curve task. In addition, this system was designed such that power is only needed during the act of pitching the blades, resulting in a higher total power delivered to the load. The overall drive train system, which transmits the power from the blades to the generator, was designed with large factors of safety in mind, such that the driveshaft and the surrounding pitch control system would be guaranteed to be operational, even at high wind speeds or other extreme conditions.

Figure 1. Side view of turbine

The design of the electrical and controls system began with the generator and focused on success within the competition tasks. To succeed in the Durability Task, the team decided that a generator that provided a high current was essential. The Maxon RE 50 was chosen as our generator as a result. For the Cut-In and Power Curve tasks, an Arduino Micro runs the finite state machine that controls the turbine. During the Control of Rated Power task, the control system implements a PID algorithm to pitch the blades to a less efficient angle at rated wind speed such that the turbine will maintain rated power and speed at higher wind speeds. In the Safety Task, the electrical system will detect either the button press or load disconnect and short the generator, creating an opposition torque that will slow the turbine down to less than 10% of rated RPM. Once the load reconnects or the button is no longer pressed, the system will detect the change and remove the short, directing power back to the load and restarting the turbine. Finally, during the Durability Task, the team designed a circuit consisting of parallel DC-DC converters to charge the supercapacitor and regulate the load voltage to 5V.

The turbine was tested six times throughout the year in the Newport News Shipbuilding Lab at Virginia Tech, operated by the Kevin T. Crofton Department of Aerospace and Ocean Engineering. The turbine was able to cut in below 4 m/s winds, and could produce a balanced power curve that provided 27 W at 11 m/s. For the Control of Rated Power and Speed Tasks, the turbine was able to pitch the blades to the angle necessary at any wind speed up to 18 m/s to maintain rated power and speed. The Safety Task operability was verified to perform as designed. The Durability Task was verified to maintain 5 V through any change in wind speed or load. The data collected during testing also verified the accuracy of the blade MATLAB model.

The turbine developed for this year's Collegiate Wind Competition was designed with the successful and safe completion of competition tasks as the primary goal. Through testing, the team has verified performance in all five of the competition tasks, giving the team confidence that the turbine will be able to perform exceptionally well at the 2019 Collegiate Wind Competition.

Section I: Blades

Blade Design

Last year's blade was designed to maximize rated power and as a result performed poorly at cut-in and low wind speed power performance. The objective for the Aerodynamics Team this year was to design a blade that balanced both cut-in and overall power curve performance. The design process consisted of three phases: airfoil selection, chord and twist design, and static performance analysis. The team used various in-house and external resources such as XFOIL, MATLAB, and QBlade to design and analyze the blades.

Airfoil Selection

Airfoil selection is crucial to balance both low and high wind speed performance. The root of the blade has a greater influence at low wind speeds and cut-in performance while the tip of the blade influences high wind speed and rated power performance. A two-airfoil design was thus chosen to maximize blade performance for these specific tasks. A variety of airfoils were analyzed in XFOIL across the expected Reynolds number range to determine the best performing airfoils. The FX 63-137 was chosen as the root airfoil because its high lift coefficient improves cut-in and the SG6043 was chosen as the tip airfoil because its high lift to drag ratio improves overall power performance. The two airfoils used in the design can be seen in **Figure 2**. The middle section of the blade is a gradual spline between the two airfoils to smooth out aerodynamic discontinuities that would be present from sudden changes in cross section.

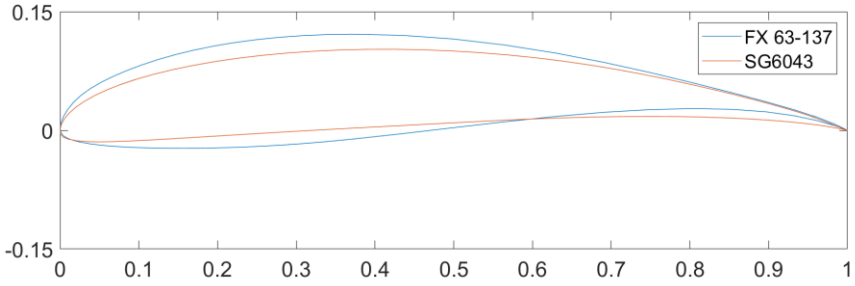

Figure 2. Cross section for FX 63-137 and SG 6043 airfoils

Chord and Twist Design

The Aerodynamics Team developed multiple in-house MATLAB programs to allow for a more customizable design process compared to using externally available open-source code. Chord and twist design was initially completed in MATLAB and finalized using QBlade. First, the team developed a Blade Element Momentum Theory (BEMT) code in MATLAB [1,2,3,4]. In combination with the BEMT code, an optimization code [5] was created to determine the initial chord and twist distribution of the blade by allowing the user to specify multiple parameters including an initial blade design to be optimized, any desired geometric constraints on the design, and the optimization objective: minimize cut-in wind speed, maximize power curve performance, or both. The code goes through a numerically implemented gradient based optimization algorithm to find the design that minimizes the objective function.

The optimization code was run several times to account for various combinations of cogging torque, chord distributions, and airfoil selection. The algorithm determined that a long chord starting at the root airfoil and gradually tapering towards the tip of the blade resulted in a similar power curve but better cut-in than any other design. Also, the spliced combination of the two airfoils performed superior to either of the airfoils alone, validating that a two-airfoil design was best. **Figure 3** shows the final chord and twist distribution that includes the cylinder and airfoil portions of the blade.

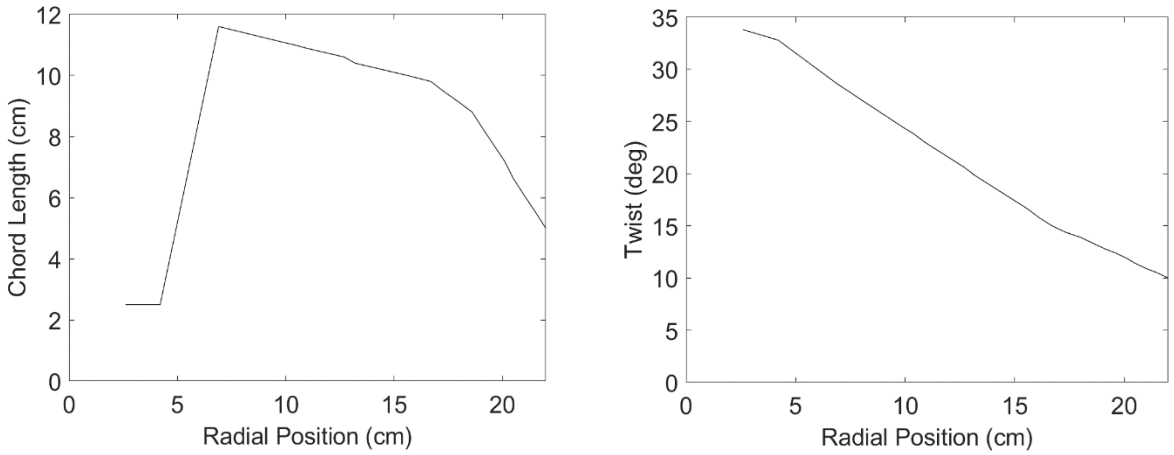

Figure 3. Chord vs. radial position (left) and twist vs. radial position (right) for final blade design

The output of the optimized geometry was input into QBlade to incorporate the cylinder portion near the root and smooth out any geometric transitions. **Figure 4** shows the final blade design.

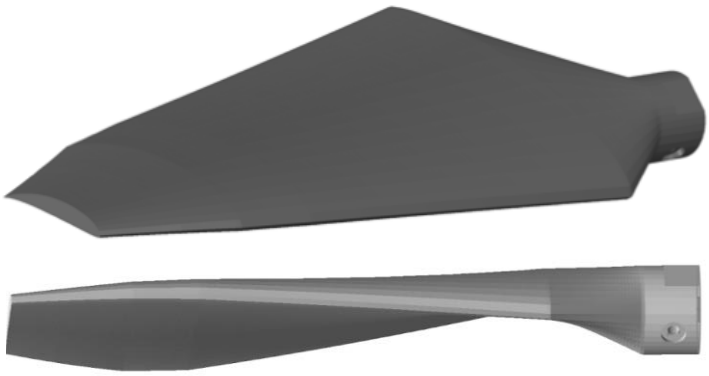

Figure 4. 3D rendering of final blade design

Static Performance Analysis

While aerodynamic analysis could have been performed with the team's in-house MATLAB code, QBlade was ultimately used because of advanced features such as interpolated airfoil data for splined sections, new tip and root loss corrections, and 3D corrections. **Figure 5** shows the static performance analysis from QBlade at 5 and 11 m/s. For both wind speeds, the maximum power coefficient occurs at a tip speed ratio between 2 and 2.5. The maximum power coefficient increases from 0.25 to 0.3 due to the increased airfoil performance at high Reynolds numbers.

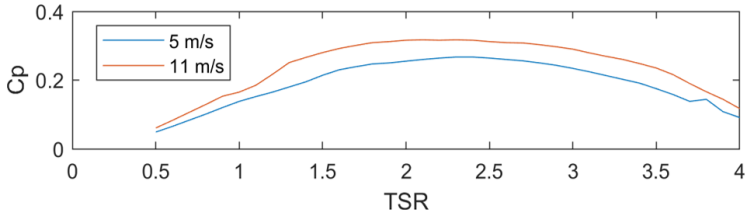

Figure 5. Power coefficient (Cp) vs. tip speed ratio (TSR) for final blade design in QBlade

Last year's turbine could not produce more than 1 W below 11 m/s. This problem was diagnosed by plotting blade power against generator power and finding that the blades produced less torque than the

generator requires at low wind speeds. To ensure that would not happen this year, blade power curves created in QBlade were graphed against generator power curves from bench testing, as shown in **Figure 6**.

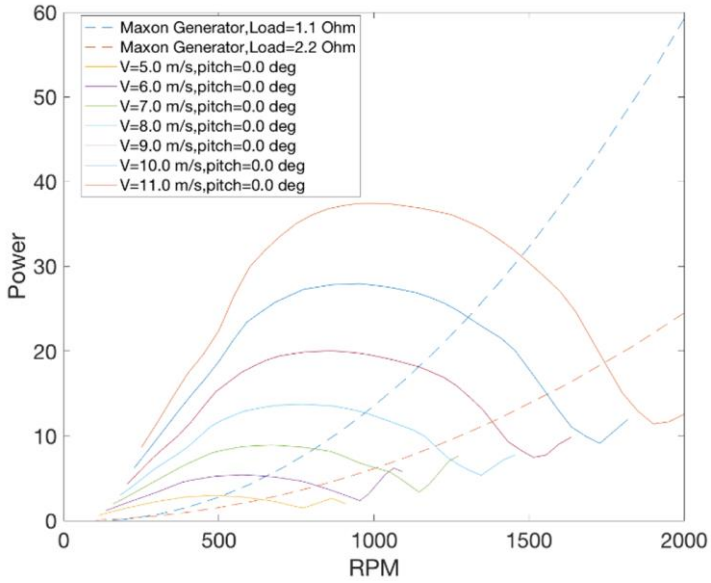

Figure 6. Blade and generator power vs. RPM

These plots showed the blades could provide enough torque to overcome the generator and spin the turbine at low wind speeds. The plots also showed the importance of selecting the appropriate generator load to best match the blade power curves. Based on available loads found during bench testing, a 1.1Ω resistance proved to be the best and the resulting turbine power curve was plotted in **Figure 7**.

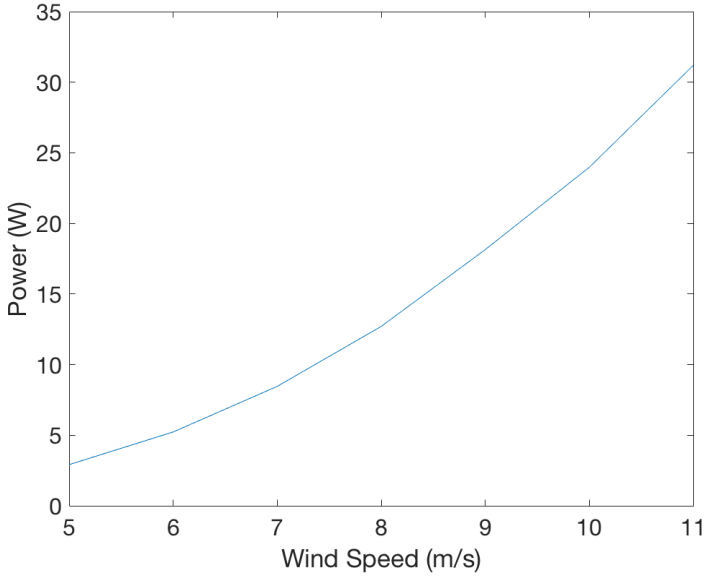

Figure 7. Predicted turbine power curve at 1.1Ω load (right)

It is important to note the assumptions that will affect the turbine's real power curve: electrical and mechanical efficiencies were approximated and the generator power curves do not take into account a torque being applied to the generator. It was found experimentally through turbine testing that a 2.2Ω resistance is best.

Blade Manufacturing

All blades, as well as several mechanical components, including the hub and nose cone, were manufactured with the use of 3D printing technology available to the team. Design complexities and the ability to rapidly prototype while maintaining favorable mechanical properties were the driving factors in this decision. Last year, negative molds of the blade design were machined and filled with an expanding foam to produce formfitting blades. Although the process was easily reproducible, fabrication was user intensive and prone to error, surface defects and inconsistencies in blade weights were common, and changes to blade dimensions required time consuming re-machining of the molds, resulting in the inability to iterate quickly. By 3D printing, the team was able to maintain structural integrity while allowing for much faster manufacturing. Early prototyping with 3D printed blades showed high dimensional accuracy with minimal defects but produced a rough surface finish constrained by the minimum thickness of each layer. This was addressed by coating the blades with Smooth-On XTC-3D finish which showed significant improvement in surface roughness. This resulted in a 55% increase in max power which produced an additional 9.4 W at 11 m/s.

The materials and build parameters were assessed for mechanical properties and dimensional capabilities. FFF printing was found to be the best candidate for fabrication, as the layer-to-layer bond strength was superior for the structural capability required to withstand the rotational loading on the blades. Model ABS-P430 material was used for its high yield strength and interlaminar adhesion. The Stratasys uPrint SE Plus printer was used to yield high resolution for preserving the complex airfoils while also allowing for minimal surface roughness prior to coating. Blades were tested through the entire expected range of wind speeds and survived, thus validating material choice. One limitation of the additively manufactured blades was the tapering of the trailing edge, which was restricted to the thickness of one filament layer height. The fragility of the edge layer impeded proper coating and was prone to fracture, so the raster orientation of the print head was modified to lay filament transversely to the leading and trailing edges of the blade. Rather than the edges of the blade comprising of a continuous trail of filament, the perimeter was defined by a pattern of hundreds of lines perpendicular to the edge. Building the edge through the adjusted settings also approximated the geometry with greater precision, as the decrease in intervals between each length of filament led to higher frequency for adjustment of the curves.

Section II: Mechanical Design

Pitch Control

Overview

At the onset of the design process, the team deliberated the merits of designing for active pitch control over the use of static blades. Although static blades would simplify the design considerably, active pitch control allows for greater turbine performance during virtually all technical tasks. It was also a creative challenge that the team unanimously coveted. Given the magnitude of this challenge, a majority of the mechanical design was dedicated to achieving consistent and reliable pitch control, as will be apparent in the coming section.

To achieve this, the team designed a system converting translational motion within the drive train into rotational motion of the blades. This was accomplished in multiple stages using a timing belt driven by a single stepper motor, two parallel lead screws, and a rack and pinion system within the hub to rotate the blades. Last year, the team's pitch control design consisted of three individual stepper motors within the hub controlling pitch. However, two major issues arose: misalignment of the blades resulting in non-uniform pitching and power losses through a slip ring. By transitioning to a single stepper motor controlling linear actuation, the blades can be pitched at the same rate and to precise angles. This consistency helps reduces vibrations and by eliminating electronics within the hub, power losses resulting from the use of a slip ring are avoided.

Linear Actuation

Figure 8 and 9 show a side view of the linear actuator and label important components. The pitching system operates by mounting a brass pinion gear on each blade **(Part 1** in **Figure 8)** and moving the blades together with three separate racks **(2)** all mounted to a singular plate **(3)**. The blades are pitched by moving the plate forward and backward relative to the fixed position of the blade spars, rotating the blades by an amount corresponding to the plate's displacement from its original position. To pitch the blades while the assembly is rotating about the drive shaft **(4)**, the plate must have the ability to rotate while simultaneously moving with linear independence. To accomplish this, the drive shaft is mounted inside an outer aluminum sleeve **(5)** that rotates with the drive shaft and can move axially along its length. To support the weight of the hub, a brass bushing is placed inside the tip of the sleeve and around the driveshaft.

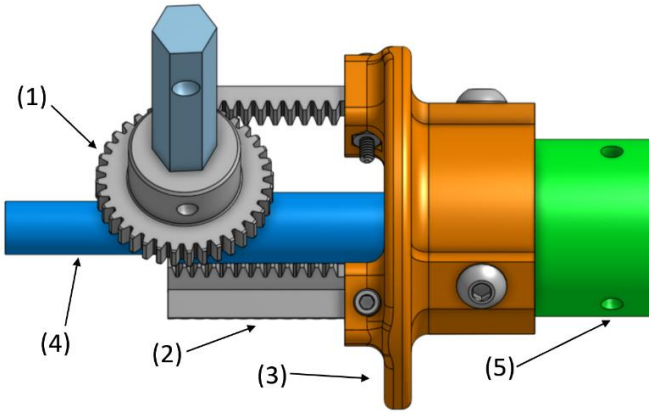

Figure 8. Side View of Hub Pitching Components

The sleeve was mounted within two radial bearings such that it could handle both compressive and tensile forces experienced during pitching while also rotating with the drive shaft. These bearings are secured in two aluminum housings **(Part 6** in **Figure 9)** and mounted on lead screws **(7)** which were positioned on either side of the housing's central bearing. As the lead screws rotate, the housings are either pushed or pulled, which transfers the motion to the racks inside the hub. This rotation is accomplished with a single stepper motor **(8)**. The stepper motor and each lead screw have a timing belt pulley **(9)** fastened to their ends, and the timing belt is routed between the pulleys to transfer the rotational motion of the stepper motor to each lead screw accurately. Additionally, the bearing housings are fastened together by an aluminum bar on their undersides, and a linear rail **(10)** was installed on the bottom of this bar. Two linear carriages were mounted to the baseplate of the turbine and the linear rail was inserted into these carriages, allowing the vertical forces and moments to be primarily carried through the linear carriage as opposed to the lead screws. This helped to prevent binding in the lead screw system. This approach resulted in several benefits. First, it allowed mechanical advantage to be gained from the lead screw pitch and the relative sizes of the timing pulleys on the stepper motor and lead screws. In addition, the stepper motor can be turned off to minimize power draw without risk of the system being back-driven.

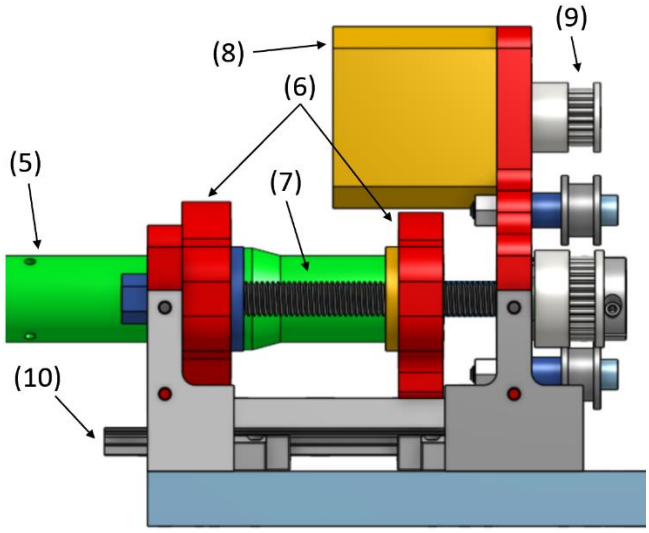

Figure 9. Drive Train Pitching Components

Rotational Spar Assembly

To translate the rotational motion of the pinion gear to the blade, an assembly was created with various components located within the hub. **Figure 10** identifies each component in the spar assembly. As a guide for the racks that rotate the pinions **(1)**, rack blocks **(2)** were designed that attach inside the hub and sit next to the spar assembly. The team chose a hexagonal spar **(3)** design over a cylindrical rod because of its ability to transfer torque more reliably and be easily assembled. The pinion gears have a single set screw

(4) located on its flange used to secure the pinion to the spar. The blade **(5)** is fixed to the spar by inserting the spar into a hexagonal hole at the root of the blade. The blade is held in place with a bolt **(6)** and secured with a lock nut **(7)**. The through hole is counterbored on the bolt head side to lay the bolt head flat, while a hex shaped counterbore appears on the nut side to fix the nut in place while tightening the bolt. To allow the blade to freely rotate about the pitching axis, the team included a radial bearing **(8)** and an adapter **(9)** to secure the hex shaft to the circular bearing. Once manufactured, initial results showed that rigidity in the spar assembly was inadequate, as the blades experienced wobbling which contributed to vibrations during testing. In response, a center support **(10)** was created and attached to the drive shaft to provide a second constraint for the spar.

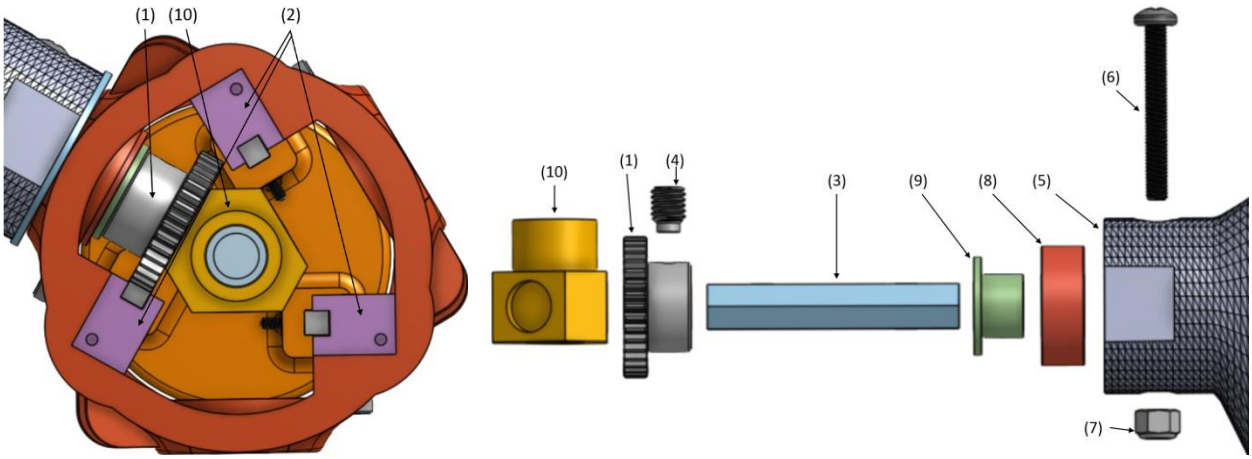

Figure 10. Internal hub components (left) and exploded spar assembly (right)

Component Overview

Sleeve

The sleeve was designed to transfer the force from the stepper motor to drive the pitch control system. The extrusion at the end of the sleeve pushes against the rear pitch control bearing during pitch retraction. The collar near the center of the sleeve pushes against the front pitch control bearing. The inner cavity contains the brass bushing that supports the drive shaft that runs through the sleeve to allow for smooth linear motion.

We performed a stress analysis using Autodesk Inventor using the estimated 21 N of backward thrust from the blades calculated with BEMT. **Figure 11** displays the results of the FEA, showing a factor of safety of 15 over the entire sleeve. Because the stress is cyclical, the endurance limit of the part had to be considered. However, aluminum does not have an endurance limit, but if we assume the turbine will experience less than 5 x 10^9 cycles, the material can handle a maximum stress of 55 MPa [6]. Given that the maximum stress the sleeve experiences is 2.082 MPa, we can safely assume that the sleeve will endure for the life of the turbine. It is important to note that while this component is significantly stronger than needed, the specific dimensions were chosen to promote easy machinability and to increase the rigidity of the system.

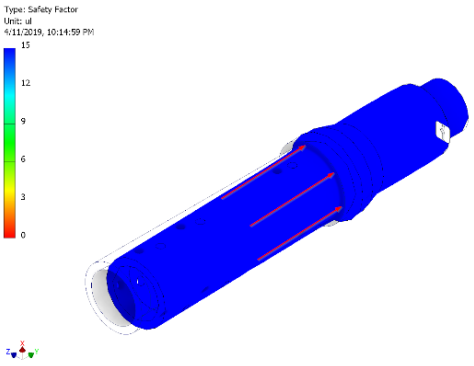

Figure 11. Sleeve FEA displaying FOS

Drive Shaft

To determine the safety factor of the drive shaft, an FEA was done on the shaft and the forces due to the hub and brass bushings were all assumed to be point loads. By measuring the weight of the hub at 300 grams, the tip force was assumed to be less than 3 N. Additionally, the maximum thrust force from the blades was found to be 21 N, and the total torque supplied to the tip of the drive shaft from the blades was calculated at 143 N-mm. The FEA was then done on the drive shaft with material properties of low carbon steel. This resulted in a minimum factor of safety of 15. The results of this FEA, as well as the position of each of the loads, can be seen in **Figure 12**. Of course, it must be noted that this was a static analysis, and the drive shaft experiences cyclical loads as the turbine blades rotate to produce power. By looking at the S-N curve of low carbon steel, the endurance limit is approximately half of the yield strength [7]. By dividing the static safety factor by two, the dynamic safety factor of the shaft was then found to be 7.5, assuming the shaft is run for infinite cycles.

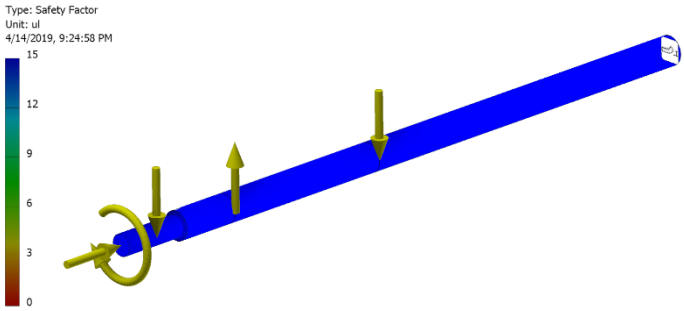

Figure 12: Driveshaft FEA

Linear Rail & Carriages

To support the aluminum sleeve and allow for axial motion, a linear rail was inserted between two offset carriages snuggly. By drawing a free body diagram assuming the sleeve, housings, and hub are all rigidly connected, we assumed the system to be a simply supported beam with two-point loads at each linear carriage, and a point load from the weight of the hub. The distributed loads from the weight of the sleeve and rail are assumed to be negligible compared to the weight of the hub. With the previously calculated hub weight of 3 N, the force on each bearing from the moment induced by this offset load can be calculated at 8.9 N and 5.9 N for the front and rear linear carriages, respectively. With each carriage capable of supporting vertical loads of 100 N, the system has an approximate safety factor of 11 [8].

Bearing Selection

The pitch control actuation system utilizes six bearings with varying functions and expected loads. All the bearings experience negligible radial loads due to the small weight of the system. Two large bearings support the sleeve, referred to as the front and back bearings. During use of the stepper motor for pitch control actuation, the face of these bearings pushes against the sleeve. The original design iteration used two linear bearings between the drive shaft and sleeve that provided support and allowed the sleeve to move concentrically over the drive shaft, which was later replaced with a low friction brass bushing to further distribute the load to allow for easier linear motion. Four bearings allow the lead screws to freely rotate and are referred to as screw bearings.

The main requirement for bearing selection is the ability to withstand high axial loads as the radial loading is well within the rating of all bearings. The maximum backwards thrust and the maximum speed experienced by the assembly were calculated to be 21 N and 2000 RPM, respectively. To meet these conditions, we selected single-row deep-groove open ball bearings, which can support greater axial loads than ordinary ball bearings. The front bearing chosen can withstand an axial load of 912.5 N, resulting in a factor of safety of 43.5, and a has a limiting speed of 12,000 RPM. The back bearing can withstand an axial load of 712.5 N, resulting in a factor of safety of 34, and has a limiting speed of 32,000 RPM. The four screw bearings can withstand an axial load of 237.5 N, with each supporting half of the thrust force from the blades, resulting in a factor of safety of 22.6. The screws will only be turned incrementally, so limiting speed is negligible. All bearings were secured by being pressure fit into their respective housings.

Stepper Motor and Lead Screws

Our team picked lead screw sizing based on several parameters from the surrounding sub-systems. Firstly, to adequately perform all tasks, the blades needed a full range of motion of 35 degrees. Additionally,

to make the hub as small as possible, the pinion gears were chosen with a pitch diameter of 2 cm. To allow this, the lead screw system needed to be capable of at least 7.0 mm of travel. Because this system would be difficult to edit later, this range was increased to 12.5 mm to accommodate any possible future changes. Based on the potential loads on each lead screw, M8-1.25 lead screws were chosen to meet the constraints.

The stepper motor selection was based off the maximum torque required to pitch the blades at 20 m/s, calculated to be 0.405 N-m at the blade spars. By assuming the lead screw friction coefficient to be between brass and steel, the maximum torque at the stepper motor was calculated at 0.189 N-m. The team selected a stepper motor with a maximum torque of 0.363 N-m, resulting in an operational margin of 1.92. Additionally, to increase the factor of safety, the timing pulley on the stepper motor was chosen to have a 33% smaller radius, thus increasing the operational margin to 2.89. The stepper motor has a resolution of 1.2 degrees per step, so when paired with the rack and pinion and pitch of the lead screws, our turbine requires 62.83 steps to pitch the blades by one degree. The small resolution of the stepper motor allows the system to have significant precision in pitch angle. To power the stepper motor, the power from the generator is passed through a buck converter such that the motor is given 4V and draws the necessary 1.2 A to pitch. These voltage and current values were found experimentally and ensure that the stepper motor will not bind at even the highest wind speeds.

Nose Cone and Hub

The nose cone is a key feature in the assembly as it transfers torque from the hub through a shaft collar and into the drive shaft itself. The spars could not be directly attached to the drive shaft due to their rotation during pitch control; therefore, the nose cone is used to transfer rotation from the hub to the drive. To strengthen the contact surface between the nose cone and the hub, aluminum rack blocks are fixed with screws through the nose cone, securing the nose cone in place. On the outer surface of the hub, dial indicator extrusions are present to more accurately align the blades during assembly. Small pointers were also 3D printed to attach to the hex spar beneath the root of the blade, allowing the team to visually estimate blade angle at any given time. Components discussed above can be found in <

Figure 13.

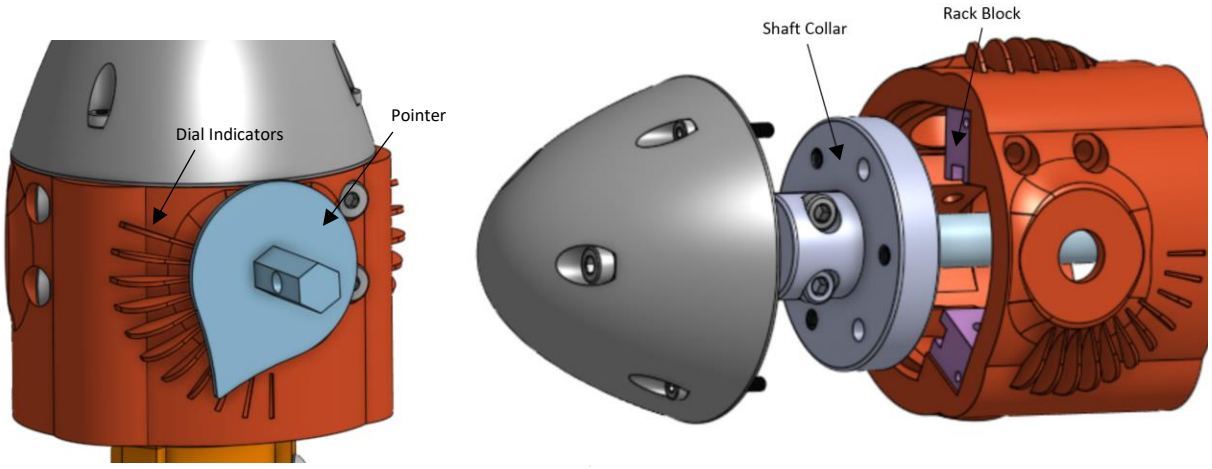

Figure 13. Dial indicator and pointer (left) and exploded hub and nose cone assembly (right)

The hub system is currently fabricated using both Polyjet 3D printing for small parts requiring intricate geometries and FFF 3D printing for structural housing components. Polyjet parts were printed on the Stratasys Connex3 using Digital ABS Plus filament. FFF parts were printed on the Stratasys Fortus 360mc using Model ABS M30 filament.

Yaw System & Tail

To achieve optimal performance of our wind turbine, we implemented a passive yaw system composed of a tail and a slewing bearing. With a maximum permissible titling moment of 100 N-m, the bearing has a safety factor of 10 at 20 m/s winds with a backwards thrust of 21 N [9]. The bearing also has a max rotatory speed of 1800 degrees per second, which exceeds the 180 degree per second requirement, making this slewing bearing assembly an ideal choice for our application.

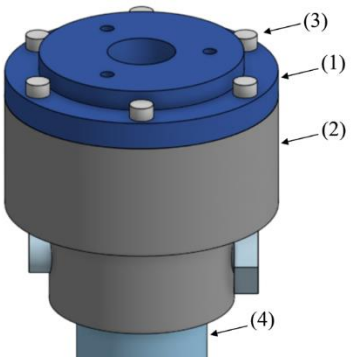

Figure 14. Yaw assembly

Our yaw assembly is made up of two main components, seen in **Figure 14:** a slewing bearing **(1)** and a yaw adapter **(2)**. The system has three bolts going through holes in the baseplate and into tapped holes in the inner ring of the slewing bearing. There are six screws **(3)** around the perimeter of the outer ring of the slewing bearing connecting into the yaw adapter, which is bolted to the tower **(4)**. This system allows our turbine to yaw effectively while compensating for additional forces.

In design of a passive yaw system, a tail of maximum surface area, shown in **Figure 15**Error! Reference source not found., is essential for keeping the turbine facing into the wind by creating the largest drag force possible. Since drag force correlates directly with area, this design allows for maximum torque to be created by the tail. The dimensions of the tail consume the rest of the 45 cm of allowable space from the nose cone to the end of the tail, with a height of 45 cm and a length of 20 cm. These dimensions give the tail a drag force of 3.59 N when facing perpendicular to a 6 m/s wind. From testing of the yaw system, it was determined that a moment of 0.15 N-m is required to overcome the internal resistance of the yaw bearing and initiate yaw rotation. Furthermore, to achieve the CWC required yaw rate of 180 degrees per second, a moment of about 0.2 N-m must be applied by the tail, which is less than the calculated yaw moment of 0.49 N-m at 6 m/s winds.

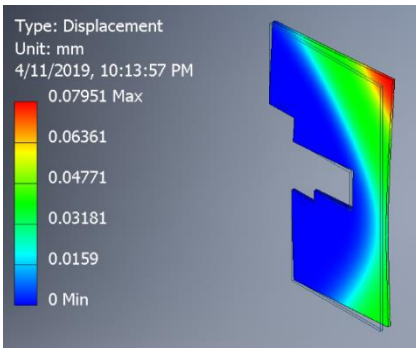

Figure 15. Tail FEA

Our team chose a 3/16” sheet of acrylic to use as the tail based on the material’s strength, rigidity, and weight. This acrylic sheet was cut with a laser cutter to maximize the surface area while staying within CWC rules and regulations. Running the worst-case scenario of the tail oriented at a 90° angle in 20 m/s winds, a maximum deflection of 0.08 mm was calculated and shown in **Figure 15.** The tail is mounted securely at two points: tied to the nacelle and fastened to the base plate with L-brackets.

Nacelle

The nacelle’s main function is to act as a smooth cover for the drive system. To achieve this, the design of the nacelle is a shell that hugs the drive and pitch actuation system. The front of the nacelle is flush with the front bearing block on the actuation system, so the blades can pitch as far back as possible. The nacelle then flows upward to accommodate the height of the total actuation system with the top rear portion of the nacelle as a mount for the tail, as seen in **Figure 16**. The nacelle was 3D printed and cast in resin due to the unusual shape and material specifications. The nacelle is subject to relatively small forces, so a 0.5 cm thickness was chosen to give the shell structure while also minimizing weight. The resin has a tensile strength of 21.5 MPa, meaning the nacelle will be able to withstand a yawing force of 116 N at the tail contact point with a factor of safety of

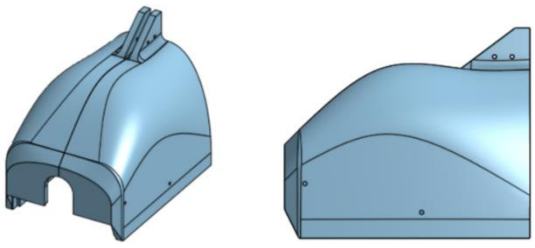
Figure 16. Nacelle rendering

10. The maximum yawing force that this system will experience is 39.9 N when perpendicular to 20 m/s wind, so this calculation is conservative.

Tower

The tower is the support structure for all turbine components and is the mounting connection to the CWC wind tunnel. Our design utilized an aluminum tube with a diameter of 3.81 cm and a wall thickness of 6.35 mm. This design allows wires to pass through it, as per CWC rules and regulations, and is adequate for our loading shown in **Figure 17.** Our team performed a stress analysis on the tower and base welded interface for the worst possible conditions at 20 m/s winds and found the stress to be 11.15 MPa when assuming the weld's fillet joint has a stress concentration factor of 2. This stress correlates to a factor of safety of 21.65 for our chosen tower geometry. This factor of safety could be lowered to allow for material savings, but the increased strength allows for the entire turbine to be built on a more rigid base and thus mitigating the effects of potential vibrations.

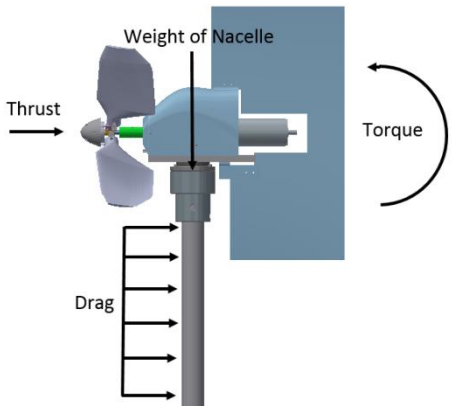

Figure 17: Turbine Loading FBD

Section III: Power Systems and Controls

Electrical and Controls Design

The electrical design focuses on power maximization, system efficiency, robustness in operational extremes, and safety in its completion of the competition tasks. **Figure 18** shows the system level layout of the entire electrical system for the wind turbine.

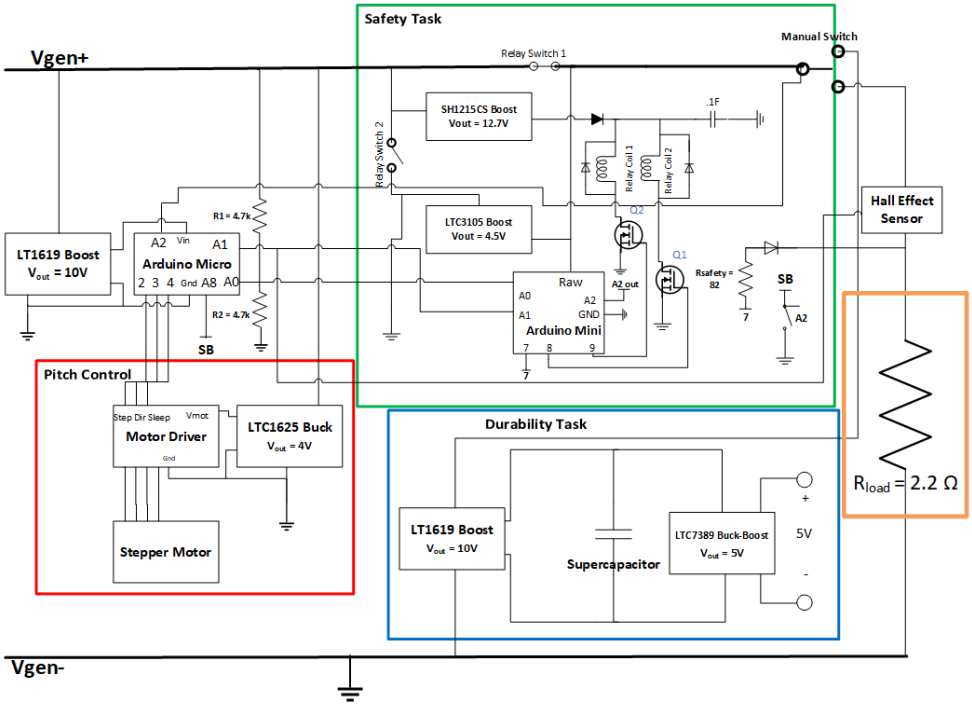

Figure 18. Wind turbine electrical system schematic

Generator Selection and Analysis

Figure 19. DC generator [10]

The team decided that a Permanent Magnet DC (PMDC) motor would be the ideal machine to use as the turbine's generator. The selected PMDC motor is the Maxon RE 50, shown in **Figure 19**. Even though AC machines are the industry standard, the team chose a DC generator over an AC generator to avoid the power loss of having a rectifier and to reduce the overall size of our system. One of the criteria for the generator was the ability to produce greater than 6 A at 11 m/s to charge the Durability Task supercapacitor. A survey of diodes on Digi-Key yields an average $V_{Forward}$ of 500 mV when the diode is rated for our application. For a rectifier, 2 diodes will be conducting during a given phase. With 6 A of current the power loss per diode is 3 W, resulting in 20% efficiency loss ($\eta = \frac{2*3W}{30W} = 20\%$) over the rectifier. With a DC generator, the rectification is done internally with a commutator. The commutator accounts for most of the efficiency loss of a DC generator but this can be vastly minimized by finding a DC generator with a low internal resistance. The Maxon RE 50 has a measured internal resistance of 0.1 Ω. The efficiency of the Maxon RE 50, assuming a 2.2 Ω load is calculated as:

$$Efficiency = \frac{P_{Load}}{P_{Total}} = \frac{R_{Load}}{R_{Internal}+R_{Load}} * 100 = \frac{2.2\Omega}{.1\Omega+2.2\Omega} * 100 = 95.6\% \quad \{1\}$$

Furthermore, using a DC generator saves space in our enclosure, as there is no need for rectifier diodes, heatsinks, and smoothing capacitors.

To avoid spending valuable time and money in the generator selection process, the team developed a Simulink model, shown in **Figure 20,** using steady state state-space equations that would allow us to determine the input-output relationships of generators using only the technical data found on the supplier's website. The state-space equations based on armature current (a), field winding currents (f), and rotor velocity (ω_r) are listed in equations {2} through {5}. P is the number of poles, τ is torque, J is rotational inertia of the machine and load, and D represents the effects of windage and friction.

$$\frac{di_a}{dt} = \frac{1}{L_a} * \left(v_a - r_a * i_a - L_{af} i_f \omega_r\right) \quad \{2\}$$

$$\tau_{electrical} = L_{af} * i_f * i_a \quad \{3\}$$

$$\frac{di_f}{dt} = \frac{1}{L_f} * \left(v_f - r_a * i_f\right) \quad \{4\}$$

$$\frac{d\omega_r}{dt} = \frac{P}{2} * \frac{1}{J} * \left(\frac{P}{2} * \tau_e - \tau_m - D * \frac{2}{P} * \omega_r\right) \quad \{5\}$$

The Maxon RE 50 was selected as the generator for the turbine because it had the lowest internal resistance of any motor the team found while also having the voltage and current characteristics to be successful. Combining equations {2} through {5} and the load power equation {6} to match the blade design, the model calculated an ideal load of 1.96 Ω, an operating speed of 1900 RPM, a current of 3.82 A with a 2.2 Ω load, and ~6 A with a large capacitive load at 11m/s wind.

$$Load\ Power\ P_L = \frac{{k_e}^2 * \omega^2 * R_L}{(R_i+R_L)^2} \quad \{6\}$$

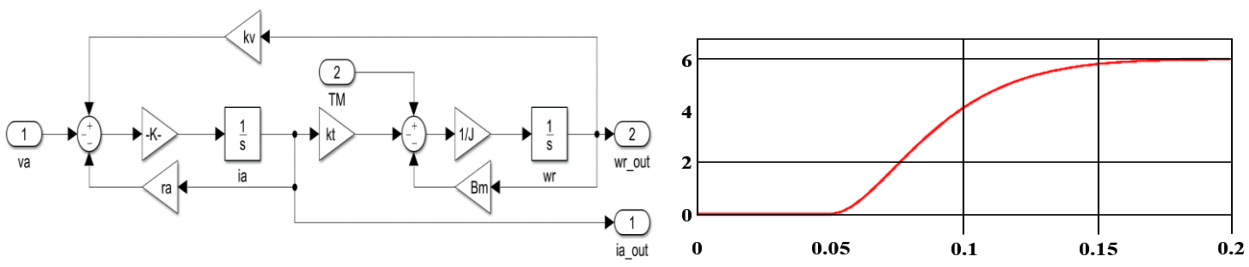

Figure 20. Simulink model of a DC generator and Current vs Time at rated conditions

When choosing the Maxon RE 50 the team weighed output power heavily to match the blade power curve. If blade power is greater than generator power for a particular RPM, the blade torque will outweigh the generator torque ensuring that the wind turbine would speed up to the designed operating point.

Arduino Micro Finite State Machine and Task Operations

The team decided on an Arduino Micro as the microcontroller to control the turbine through the 5 CWC tasks due to its low power dissipation of 0.2 W. **Figure 21** shows the finite state machine that describes the decision-making process used by the Arduino Micro. The specific operations of each task and the conditions necessary to change states are described in **Table 1**. The Micro is biased at 10 V by the LTC1619 boost converter.

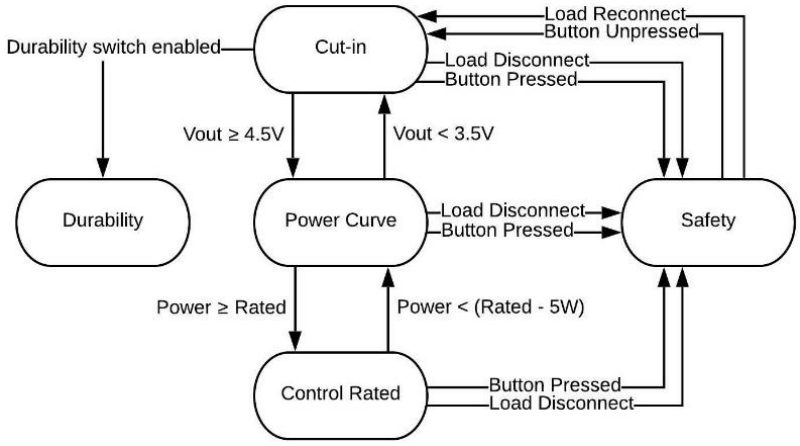

Figure 21. Arduino micro finite state machine diagram

Table 1. Finite state machine operations and state change conditions

State	Description and Functions of State	State Change Conditions
Cut-in	• Default state when Arduino turns on. Blades in cut-in position • Take measurements and make decisions from this state	• Safety task button pressed or load disconnected, go to safety state • Durability task switch flipped, go to durability state • Load voltage > 4.5V, go to power curve state. ○ 4.5V is when the motor driver is properly biased

Power Curve	• Pitch blades from current angle to power angle
	  ○ Distance between the cut-in and power angles is 4.5°
	  ○ PID controller tracks changes in pitch
	• Maximizes power generated at wind speeds under 11m/s
		• Safety task button pressed or load disconnected, go to safety state
		• Durability task switch flipped, go to durability state
		• Output power > rated power, go to control rated state
		• Output voltage starts dropping under 4V, back to cut-in

Control Rated	• Run PID controller to maintain rated power by pitching the blades ○ Rated power is pre-determined through testing	• Safety task button pressed or load disconnected, go to safety state • Durability task switch flipped, go to durability state • Output power drops significantly under rated, back to power curve

Safety	• Immediately pitch blades to cut-in angle for easy re-start after safety task • Use generator braking protocol	• Safety button un-pressed, go to cut-in • Load is reconnected, go to cut-in
Durability	• If output power > rated power, run PID controller to maintain rated power ○ Otherwise keep blades at power angle	• Durability switch un-flipped, go to cut-in

Measurement and Sensing

The Arduino Micro measures voltage and current as described in this section to know when to perform its control operations. The voltage across the load is scaled to the Arduino with a voltage divider and the Arduino keeps track of the voltage using a rolling average of the last eight voltage measurements to mitigate the effects of noise. The current through the load is measured by a hall-effect sensor in series with the load, which outputs a voltage that the Arduino can measure and track through another rolling average. The normally closed safety switch is connected between the 5 V pin on the Arduino and a digital pin (8), with a 2.2 kΩ pull-down resistor to ground. The digital pin then reads high for normal operation, but when the switch is opened, the pin is pulled low by the resistor. A load disconnect is detected by the Arduino constantly looking for a non-zero voltage at the output but near zero current, which implies the absence of a load.

Arduino Micro PID Controller (Control of Rated Power and Speed)

The team designed a feedback controller to control rated power above 11 m/s. The controller compares the measured power to the rated power at 11 m/s and adjusts the pitch using the PID controller algorithm shown in equation {7} where θ is the pitch, e is the difference between power and rated power, and K_P, K_D, and K_I are gain constants.

$$\theta(t) = Kp * e(t) + Kd * \frac{de(t)}{dt} + Ki * \int_0^\tau e(t)\, d\tau \quad \{7\}$$

To easily choose gains analytically, the team used a simple model that assumes a constant generator load and ignores the drive shaft. The model is shown in equations {8} through {9}, where ω is the angular velocity of the turbine, J is the rotational inertia, T_a is the torque produced by the blades, T_g is the torque produced by the generator, V is wind speed, θ is the pitch angle, η is the efficiency from electrical and mechanical losses, and P is the power output of the generator.

$$\frac{d\omega}{dt} = \frac{1}{J} * \left(Ta(\omega, V, \theta) * \eta - Tg(\omega)\right) = f(\omega, V, \theta) \quad \{8\}$$

$$P = h(\omega) \quad \{9\}$$

Linearizing this model at a wind speed, pitch angle, and rotational speed design point yields equations {10} and {11} with constants $a = \frac{\delta f}{\delta \omega}$, $b = \frac{\delta f}{\delta \theta}$, and $c = \frac{\delta h}{\delta \omega}$.

$$\dot{\omega} = a * \omega + b * \theta \quad \{10\}$$

$$P = c * \omega \quad \{11\}$$

Finally, a closed loop transfer function was derived by taking the Laplace transform of equations {7} through {11} that relates the power output of the turbine to the rated power output, shown in equation {12}. By choosing K_P, K_I, and K_D, the denominator of this transfer function can be tuned to achieve the desired response.

$$\frac{P}{P_{rated}} = H = \frac{cb(Ki + sKp + s^2 Kd)}{(cbKd+1)s^2 + (cbKp - a)s + cbKi} \quad \{12\}$$

The benefit of choosing a simple model is that it resembles a second order response equation {13}.

$$s^2 + 2\xi\omega s + \omega^2 \quad \{13\}$$

The damping ratio, ξ, and natural frequency, ω, can be defined by specifying a settling time of 10 seconds and a maximum overshoot of 1% which then inform the values of K_P, K_I, and K_D. These high-performance values were chosen to account for the expected decrease in performance from ignoring dynamics and to ensure that the turbine would settle at rated power well within the requirements of the competition. The model was linearized and tuned with this method at 12, 15, and 20 m/s and the gains were simulated in a non-linear Simulink model. The response of the model is shown in **Figure 22**. This simulation includes model non-linearities such as a lookup table for aerodynamic data from QBlade and generator data from testing, along with microcontroller non-linearities, such as delay and simulated sensor noise.

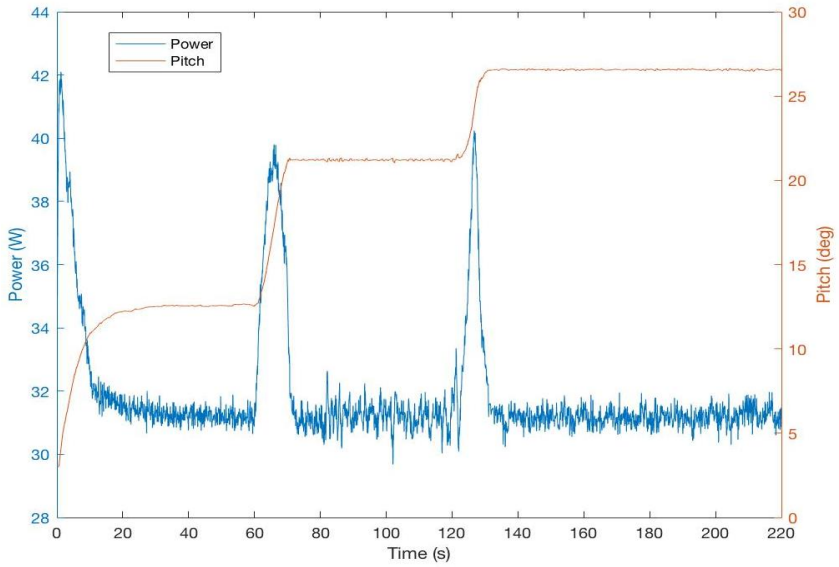

Figure 22. Predicted turbine response to constant wind speed disturbances of 12,15, and 20m/s

Turbine Safety System via Generator Braking (Safety Task)

Shown in **Figure 23** is the generator braking system that is used to complete Safety Task. The Arduino Mini's sole purpose is to look for the Safety Task conditions using voltage, current, and button press measurements. When one of the two safety task conditions are met, either the button press or load disconnect, the Arduino Micro will pitch the blades back to the cut-in angle to slow its rotation. Immediately after the Micro is done pitching the blades, a latching relay triggers to short the generator. Shorting the generator produces a large opposition torque which instantly slows the turbine down. The torque is a result of the increased strength of a magnetic field proportional to the current flowing back into the generator that opposes the rotation of the armature due to Lenz's law.

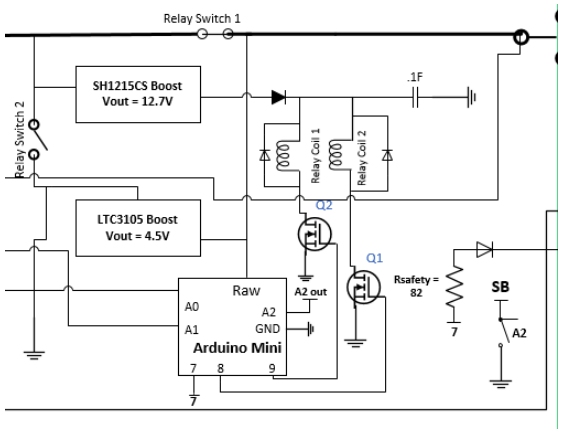

Figure 23. Arduino Mini Safety Task Circuit

Safety Task is done electrically because the electrical system will respond faster than the mechanical system and performs more consistently at high wind speed conditions. A latching relay is chosen because it only consumes power when it is being switched and consumes no power during regular operation. The latching relay is a double pole single throw (DPST). Switch 1 of the DPST connects the normal operation power path while Switch 2 is open. Switch 2 closes to short the generator, opening Switch

1, isolating the Mini and load from the main path. Switch 2 also connects the Mini to the LTC3105 boost converter which biases the Mini at 4 V using the ~0.6 V generated over the short as the input, allowing for an indefinite hold of Safety Task. The Mini cannot provide enough current to trigger the latching relay, so two eNMOS amplifiers are used to trigger the relay. Pin 9 and Q2 trigger the latching relay to short the generator while Pin 8 and Q1 unlatch the relay, releasing the short. The eNMOS are biased by three 33,000 µF capacitors in parallel (0.1 F) that are biased at 12 V by a DC-DC converter and are charged during normal operation. The two eNMOS consume little power so the 0.1 F capacitor only loses 3 V out of the stored 12 V to switch and whenever the short is released the capacitors charge back to 12 V. A diode is placed in front of the capacitor to prevent discharge through the short. The short can be un-triggered by the Mini detecting a button press to indicate safe operation. To detect a reconnect, a test voltage is sent by the Mini to the location of the load. If the load is absent, no current from the Arduino will be drawn. If the load is reconnected, current will be drawn from the Mini, which will be detected by a hall-effect sensor and the short will be released. An 82 Ω resistor is put in series with the Mini to prevent a large current draw, which could break the Arduino. A diode is used to make the 82 Ω resistor disconnected from the power path during normal operation.

Supercapacitor Charging Circuit with Output Voltage Regulation (Durability Task)

The Durability Task circuit is highlighted in blue in **Figure 18** and shown in **Figure 24.** When the manual switch is flipped, this circuit will be enabled. The LT1619 boost converter is set to charge the 58 F supercapacitor to 10 V while the LTC3789 buck-boost converter is set to regulate the output voltage to 5 V using the supercapacitor as its input. The LT1619 will stop charging the supercapacitor once 10 V is reached, ensuring the supercapacitor does not exceed its voltage rating. The LT1619 has a low threshold voltage of 1.9 V allowing for supercapacitor charging under low wind conditions. The input range of the LTC3789 is 4 V to 38 V [11], allowing us to not only step down the supercapacitor voltage, but step up the supercapacitor voltage in the event the supercapacitor falls below 5 V. Furthermore, the LTC3789 utilizes current mode control which results in faster output voltage regulation. This is important for Durability Task because the wind, yaw, and load conditions can change rapidly. Because the inductor current rises with a slope determined by V_{in}-V_{out}, current mode control can immediately respond to changes in any lines or the load [12]. Both the LT1619 and LTC3789 have current limiting options which the team set to a ~8 A. If there is a sudden turbine acceleration or electrical fault at the load, the turbine electronics will be protected from any massive surges in currents.

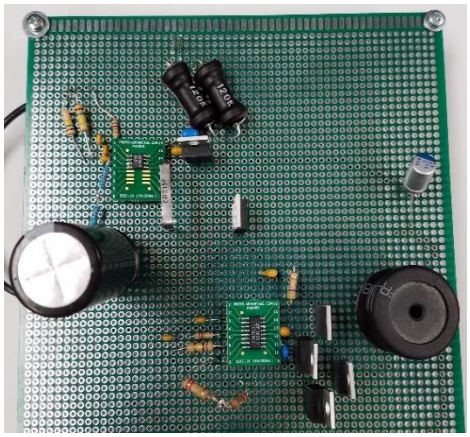

Figure 24. Power Electronics

The team opted to choose integrated circuits over making our own Arduino Controlled Converters for three reasons. (i) The integrated chips act independently of the Arduino, still charging the supercapacitor and regulating the output voltage even if the Arduino shuts off. (ii) Discrete converters with an Arduino would limit the available safety features. The LT1619 and LTC3789 come with UVLO (under voltage lockout), short circuit protection, and current limiting in a 3x3 mm^2 package. These features would be expensive and inefficient to implement with an Arduino. (iii) Using an Arduino controlled DC-DC converter would force us to use voltage-mode control. Voltage-mode control is slow since changes in the line or load would have to be sensed as a change in output voltage. Changes during durability task can happen rapidly so a fast response is desired which can be achieved with current-mode control offered by integrated circuits.

The success of Durability Task is directly tied to generator selection. The Maxon RE 50 has a high current characteristic allowing for fast charging of the supercapacitor during the minute charging period. Charging the capacitor to 10 V in one minute is unrealistic at this scale, so 6.5 V was chosen. The current

from the generator required to charge the supercapacitor to 6.5 V in one minute is shown in equations {15} through {17}.

$$Energy\ E = .5 * C * V^2 = .5 * 58 * 10^2 = 1225J \quad \{15\}$$

$$Charge\ Q = \frac{2*E}{V} = \frac{2*1225J}{6.5V} = 376\ C \quad \{16\}$$

$$Current\ I = \frac{Q}{t} = \frac{376\ A{\cdot}seconds}{60\ seconds} = 6.2A \quad \{17\}$$

The Maxon RE 50 meets the required calculated current specification, further validating our choice.

Section IV: Testing Results

BEMT Model Validation

Two blade designs were tested in the open jet wind tunnel: the final design and a similar design with a shorter chord length. The latter was used to collect power curve data to compare to QBlade's prediction. Data was collected from the cut-in wind speed of 7 m/s to the rated power wind speed of 11 m/s at a pitch of 1.5 degrees and a load of 2.2 Ω. QBlade predictions were plotted against the experimental data under the same conditions. As seen in **Figure 25**, the experimental data supported the QBlade model.

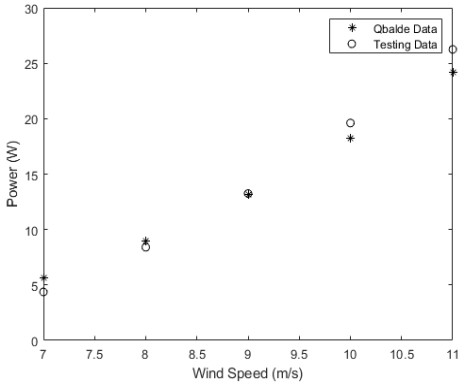

Power Curve

Shown in **Figure 26** is the generated power curve from testing. The final design was chosen over the short chord length blades because they give a better cut-in at well below 5 m/s and a more balanced power curve. The ideal load of 2.2 Ω and cut-in angle of 4 degrees were chosen because it allowed the turbine to generate enough power to pitch to a more efficient power angle between 7 and 8 m/s winds. Rated power of the system was found to be 27 W.

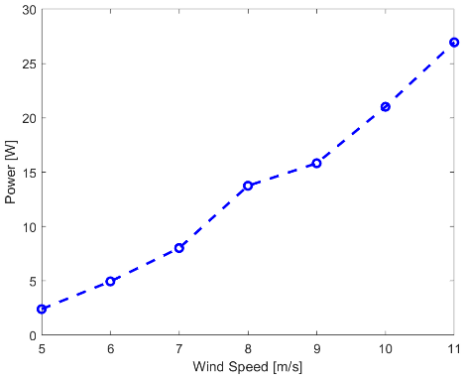

Figure 26. Power curve at 2.2 Ω load

Control of Rated Power and Speed

The turbine was subjected to wind speeds ranging from 12 m/s to 20 m/s during testing. The PID controller was able to correct the output power to rated power in approximately 30 seconds at wind speeds less than 18 m/s. Above 18 m/s, the output would oscillate around rated power without converging. To address this, the algorithm was changed for the blades to pitch in the opposite direction, back towards the cut-in. Pitching in this direction will make the power response less sensitive to small changes in pitch. This algorithm was unable to be verified at all wind speeds before the competition but was demonstrated to be viable up to 20 m/s by manually pitching the blades.

Safety Task

While the turbine was operating at 11 m/s, the button press was simulated, activating the generator safety short. This caused the RPM to drop to 10.6% of rated RPM. To pass Safety Task, the algorithm was modified to first pitch the blades back to the cut-in angle to meet the requirements. When the button was

released, the turbine restarted. The load was also disconnected and verified that the turbine could slow down and pass this section of Safety Task.

Durability Task

After one minute, the supercapacitor charged to 6.4 V under the same testing conditions expected at the competition. This was very similar to our calculations shown in Section III. Regardless of the wind speed, yaw, or load, the power electronics system regulated a steady 5 V at the load.

References

[1] Kulunk E, *Aerodynamics of Wind Turbines, Fundamental and Advanced Topics in Wind Power*, New Mexico Institute of Mining and Technology, 2011.

[2] Maheri A, Noroozi S, Toomer C, Vibbey J, *Damping the fluctuating behaviour and improving the convergence rate of the axial induction factor in the BEMT- based rotor aerodynamic codes*, University of the West of England, 2006.

[3] Ning S A, *A simple solution method for the blade element momentum equations with guaranteed convergence*, National Renewable Energy Laboratory.

[4] Shen W Z, Mikkelsen R, Sorensen J N, *Tip Loss Corrections for Wind Turbine Computations*, Department of Mechanical Engineering, Technical University of Denmark, 2005.

[5] Arora J S, *Introduction to Optimum Design*, 2017.

[6] J. E. Shigley, J. K. Nisbett, & R.G. Budynas, *Shigley's Mechanical Engineering Design*. New York: McGraw-Hill Higher Education, 2006.

[7] J. Keisler, O. K. Chopra, and W. J. Shack, "Fatigue Strain-Life Behavior of Carbon and Low-Alloy Steels, Austenitic Stainless Steels, and Alloy 600 in LWR Environments," Argonne National Laboratory, Aug. 1995.

[8] McMaster-Carr, "Sleeve Bearing Carriage Zinc, for 9 mm Wide Rail, 20 mm Wide," Datasheet.

[9] Igus, "iglide slewing ring, PRT-01, aluminum housing, sliding elements made from iglide J," Datasheet.

[10] "RE 50 Ø50 mm, Graphite Brushes, 200 Watt," *maxon*. [Online]. Available: https://www.maxonmotorusa.com/maxon/view/product/motor/dcmotor/re/re50/578296

[11] Linear Technology, "LT1619 Low Voltage Current Mode PWM Controller," 1619fa datasheet.

[12] Linear Technology, "LTC3789 High Efficiency, Synchronous, 4-Switch Buck-Boost Controller," 3789fc datasheet.

[13] Dr. Robert Mammano, "Switching Power Supply Topology Voltage Mode vs. Current Mode," Texas Instruments Design Note, 1999.

[14] Meeting with Dr. Jeffrey Mayer, Collegiate Associate Professor at Virginia Tech, Bradley Department of Electrical and Computer Engineering.